

## 1 **Ball-milled Al-Sn alloy as composite Phase Change Material**

2  
3 Chiara Confalonieri<sup>a\*</sup>, Aldo Tommaso Grimaldi<sup>a,1</sup>, Elisabetta Gariboldi<sup>a</sup>

4 <sup>a</sup>Politecnico di Milano, Department of Mechanical Engineering, Via La Masa 1, 20156  
5 Milan (Italy)

6 [chiara.confalonieri@polimi.it](mailto:chiara.confalonieri@polimi.it), [aldo.tommaso.grimaldi@mi.infn.it](mailto:aldo.tommaso.grimaldi@mi.infn.it), [elisabetta.gariboldi@polimi.it](mailto:elisabetta.gariboldi@polimi.it)

7 \*corresponding author

### 8 **Abstract**

9 The present study concerns a fully metallic solid-liquid composite Phase Change Material  
10 based on an Al-Sn Miscibility Gap Alloy produced by powder metallurgy, including its ball-  
11 milling, compression and further sintering heat treatment. The materials obtained by  
12 different routes display a narrow melting temperature range at about 230°C, corresponding  
13 to the phase transformation of Sn- or of Sn-rich eutectic. The microstructures obtained by  
14 this manufacturing process lead to form-stable PCMs, which can keep their shape and  
15 prevent active phase leakage in service conditions. Ball milling of metal powders as mixing  
16 technique allowed to obtain a very fine microstructure, resulting in stability of thermal  
17 response and improvement of mechanical properties. Among the investigated Al-40Sn  
18 mass% samples, the most promising were those compressed at 240°C followed by  
19 sintering at 500°C.

20  
21 **Keywords:** metallic Phase Change Materials; form-stable; ball milling; thermal stability;  
22 microstructure; mechanical behavior.

### 23 24 **1. Introduction**

25 Phase Change Materials (PCMs) are materials in which a phase transition occurs under  
26 specific conditions and causes a significant change in at least one material property.

27 Considering thermal properties, they can be applied as Thermal Energy Storage (TES)

---

<sup>1</sup> Present address: Istituto Nazionale di Fisica Nucleare (INFN) – Laboratorio Acceleratori e Superconduttività Applicata (LASA), Via Fratelli Cervi 201, 20090 Segrate (Milan, Italy)

1 systems, storing the latent heat associated to the phase transition. This approach is  
2 referred as latent heat storage (LH TES) and Kuta et al. [1] consider it as the most efficient  
3 way to store thermal energy; in facts, according to Fiedler et al. [2], this approach allows to  
4 store a higher energy density using less material. PCMs can be applied in several different  
5 fields. Kuta et al. [1] reported PCM-based building envelopes, which can keep proper  
6 internal conditions storing or releasing energy depending on external conditions, thus  
7 reducing the use of air conditioning or heating. Navarrete et al. [3] proposed to use self-  
8 nanoencapsulated metal/metal alloys to enhance thermal property of a Heat Transfer  
9 Fluid, obtaining a nanofluid. Considering solar energy sector, Reed et al. [4] developed a  
10 C-(Al-Si) system to be applied in concentrated solar power plants. In addition, Nazir et al.  
11 [5] reviewed many other applications, like thermal management in photovoltaic cells, smart  
12 textiles and cooling systems in electronic devices.

13 According to Sun et al. [6], the most important properties of PCMs for TES are the  
14 transition temperature and the latent heat associated to the transition; at the same time,  
15 good thermal stability and reliability of thermal performance. Moreover, Wei et al. [7]  
16 mentioned as desired properties also high thermal conductivity, high specific heat and high  
17 density. For some applications, also good mechanical properties could be required.

18 Although every phase transition (gas-liquid, solid-gas, solid-liquid, solid-solid) could be  
19 exploited to store energy, usually only solid-solid and solid-liquid transition are applied,  
20 due to the large volume changes associated to gas transitions. Among them, solid-liquid  
21 transitions have generally higher latent heat with respect to solid-solid ones; however, the  
22 liquid phase needs to be enclosed in some way to avoid leakage. The main properties of  
23 potential PCMs based on solid-liquid transition are shown in Table 1. Among the wide  
24 range of materials that have been considered as PCMs for TES and, more in general, for  
25 thermal management of systems, metallic PCMs are so far the less developed class;  
26 Mohamed et al. [8] ascribed this fact to their low heat of fusion per unit weight.

Commentato [CC1]: In questa frase ho tolto i riferimenti perché venivano male inseriti su cose abbastanza ovvie

Commentato [CC2]: Su et al., 2015

Commentato [CC3]: Pielichowska and Pielichowski, 2014

Commentato [CC4]: Su et al., 2015

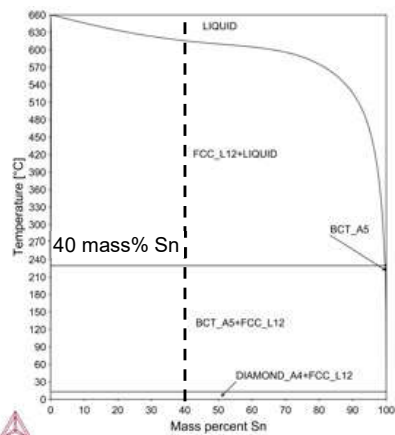
1 Nevertheless, as highlighted by Zhou and Wu [9], they have higher operative temperature  
 2 ranges (including phase transition) which makes them suitable for high-temperature  
 3 applications. Moreover, they have higher latent heat per unit volume, which makes them  
 4 attractive for compact devices.

Active Phase	PCM type	Transition temperature	Density	Latent heat		Reference
				per unit mass	per unit volume	
		°C	g/cm <sup>3</sup>	J/g	J/cm <sup>3</sup>	
Paraffin (C <sub>29</sub> H <sub>60</sub> )	organic	63,4	0,81	239	193	[10]
MgCl <sub>2</sub> •6H <sub>2</sub> O	inorganic	117	1,57	167	262	[11]
Sn	metallic	232	7,29	59	430	[12]
Cu	metallic	1085	8,93	205	1831	[12]

5 *Table 1. Main properties of some potential solid-liquid PCMs*

6 In addition to the 'classic' goals of maximizing thermal response and stability, the design of  
 7 metallic PCM can be based on the possibility to exploiting the structural properties typical  
 8 of metals. Metallic solid-liquid PCMs are usually produced by encapsulation of the active  
 9 phase in a passive-phase capsule, whose size ranges from millimetres to nanometres.  
 10 However, Zhou and Wu[9] highlighted that encapsulated PCMs may oxidize or deteriorate  
 11 particularly at high temperatures, reducing durability and energy storage performance;  
 12 moreover, Pielichowska and Pielichowski [13] observed that encapsulation process can be  
 13 complex and expensive.  
 14 To overcome these issues, Zhou and Wu [9] suggest to use of solid-solid PCMs. Another  
 15 viable alternative is the choice of alloys which behave as form-stable PCMs (FS-PCMs),  
 16 i.e. materials in which the active phase (the actual PCM) is embedded in a higher-melting  
 17 passive matrix, which remains solid at all stages preventing leakage and keeping structural  
 18 properties, as defined by Pielichowska and Pielichowski [13]. According to Sugo et al. [14],  
 19 thermal energy storage at high temperature is most efficient and compact using two-phase  
 20 mixtures in which phases are completely immiscible at solid state: in this way, it is possible  
 21 to prevent the formation of solid solutions or intermetallics, keeping the composition of the

1 two phases stable over time or with thermal cycles. So, Sugo et al. [14] suggested that  
 2 alloys with these features can be obtained exploiting miscibility gaps in phase diagrams  
 3 and so they are called Miscibility Gap Alloys (MGAs); examples of MGAs are Al-Sn, Fe-Cu  
 4 and Fe-Mg alloys. Among them, Sugo et al. [14] recommended Al-Sn based alloys as one  
 5 of the metallic systems to be applied as PCMs for high temperature energy storage,  
 6 characterized by activation temperatures close to 230°C (232°C for pure Sn).  
 7 Al-Sn based alloys are often used as bearing alloys, thanks to their excellent tribological  
 8 properties; the target microstructure for this application [15] is similar to the one desired for  
 9 metallic PCMs. A previous study on PCMs by Gariboldi and Perrin [16] focused on an Al  
 10 alloy with 20% volume content of Sn, which corresponds to about 40% mass content; the  
 11 same alloy composition was considered in this paper, as shown on the Al-Sn phase  
 12 diagram in Figure 1. This Sn content is higher than in bearing alloys, which is usually lower  
 13 than 30 mass%; for example, Liu et al. [15] used 20% mass of Sn and Noskova et al. [17]  
 14 used 30% mass. The goal of the study was to verify if it is possible to use well-known and  
 15 proven industrial processes for bearing alloys also to produce FS-PCMs.



16  
 17 *Figure 1. Al-Sn phase diagram with considered composition (computed using Thermo-Calc*  
 18 *Software TCAL6 Aluminium-based alloys database, accessed 9 January 2019)*

1 In practice, it is not so trivial to obtain the target microstructure, since natural cooling  
2 results in an opposite structure (matrix surrounded by active-phase particles). Among the  
3 possible solutions listed by Liu et al. [18], powder metallurgy is a group of manufacturing  
4 techniques which allows to obtain MGAs with "inverse microstructure". The process  
5 involves mixing, compression and finally sintering of powders; in this way, the matrix  
6 material can form a continuous body which completely encapsulates the active phase,  
7 preventing leakage in operative conditions. As a matter of fact, the resultant morphology of  
8 the active phase depends on the initial shape and size distribution of the powdered  
9 components, as well as on process parameters. In the abovementioned previous study by  
10 the research group [16], relatively fine Sn powders were simply mixed. Ball milling (BM) is  
11 the most common comminution technique to obtain fine particles from solids and it is often  
12 used in the production of bearing alloys. When a mixture of metal powders is subjected to  
13 ball milling, powder particles are mixed and reduced in size at the same time, resulting in a  
14 homogeneous alloy; therefore, the whole process is called Mechanical Alloying [19]. The  
15 expected difference between simple mixed and ball milled microstructures was a finer  
16 structure. Nonetheless, ball milling is more complex and expensive than simple mixing  
17 process. A preliminary check on ball-milling production route by Confalonieri et al. [20]  
18 suggested promising microstructures, independently on the size-distribution of Sn powders  
19 adopted. The innovative feature of the research presented in this paper is the insertion of  
20 ball milling of Sn powders into an overall production cycle to obtain FS-PCMs.  
21 Compression as well as sintering temperatures were selected as parameters of these  
22 process stages. Their effect on microstructures, thermal response and mechanical  
23 properties of the FS-PCMs was investigated before and after simulated service, to check  
24 the material properties stability.

25

26

## 1 **2. Materials and experimental procedures**

2 Two Sn powders and an Al powder were selected for the present investigation. The Al  
3 powder was an atomized high purity Al (> 99.7 mass%) powder with diameters smaller  
4 than 45  $\mu\text{m}$  (ECKA Granules GmbH, Germany). The two types of Sn powders  
5 (Metalpolveri S.r.l) having different particle size and distribution were considered: powder  
6 SN (Sn > 99.9 mass%), characterized by very fine particle-size distribution and good  
7 homogeneity, and powder 106 (Sn > 99.7 mass%), characterized by coarser particles with  
8 lower homogeneity. The second one has both a relatively high amount of fine particles (<  
9 20  $\mu\text{m}$ ) and coarse particles (anyway, generally smaller than 100  $\mu\text{m}$ ). Either powder SN  
10 or powder 106 was mixed to Al powder to get nominal volumetric composition of the alloy  
11 equal to 80% Al and 20% Sn (corresponding to about 40 mass% Sn, as shown in Figure  
12 1).

13 Each Al/Sn mixed powder was ball-milled using a planetary mill (Retsch PM 400 Planetary  
14 Ball Mill), which consists of four grinding jars that are arranged eccentrically on a sun  
15 wheel and rotate in the opposite direction with respect to it (speed ratio 1:2.5). Each Al-Sn  
16 mixed powder was sealed in stainless steel jar together with hardened steel balls  
17 (diameter 20 mm) in a ratio of 1:5 in order to have at least about 33% of empty space in  
18 the jar to assure an effective mixing. Ethanol was added as lubricant (4% on the total  
19 weight of powders) in order to avoid cold fusion phenomena. Protection from oxidation was  
20 achieved using a pure Ar atmosphere. Grinding process was conducted for 24 hours at  
21 250 rpm; to avoid excessive increases in temperature due to friction and to further  
22 minimize oxidation phenomena, grinding cycles of 20 minutes were alternated to pause  
23 cycles of 10 minutes.

24 Then, ball-milled powders were compressed into cylindrical samples and sintered following  
25 the same parameters and procedures applied in the previous research on simple mixed  
26 powders [16]. Conversely to the case of bearing alloys, in which samples are usually

1 compressed at room temperature (i.e. cold compression, technique that had been checked  
2 by Confalonieri et al. [20]), compression was conducted at relatively high temperature (hot  
3 compression, HC), just below and above Sn melting temperature (about 232°C), i.e. at  
4 220°C (HC220) and 240°C (HC240). In both cases, about 23 g of ball-mixed powders  
5 were compressed using an Instron 1195 Universal Testing Machine equipped with an  
6 extrusion set consisting of a hollow cylinder steel die and a 15 mm diameter punch; the die  
7 temperature was controlled by means of an induction heater (AHD Millennium 3-120-100  
8 Inductor Heat Generator) whose coils surrounded the die. To assure a good densification,  
9 compression was divided into three steps: pre-compression up to 20 kPa, compression up  
10 to maximum pressure, i.e. 340 MPa, and, after a pause of 60 s to allow relaxation of the  
11 structure, final compression up to maximum pressure. In this way, samples with diameter  
12 of 15 mm and height of about 18 mm were obtained. Concerning heat treatments, fractions  
13 of the samples were sintered for 1 hour in pure Ar atmosphere at 250°C, which is a usual  
14 temperature for bearing alloys, or at 500°C, as proposed for PCMs by Sugo et al. [14]. At  
15 the end of the heat treatment, samples were slowly cooled down to room temperature in  
16 the furnace, keeping the Ar atmosphere. Then, to simulate service the samples were  
17 subjected to 100 thermal cycles in air at 20°C/min between 175°C and 285°C, thus  
18 including the melting/solidification temperature range of the active phase.

19 The material characterization in different manufacturing, heat treatment or simulated  
20 service conditions included microstructural, thermal and mechanical features. X-ray  
21 diffraction (XRD) analysis was carried out at room temperature using Panalytical X'Pert  
22 PRO MPD X-ray diffractometer ( $\theta$ - $\theta$  geometry, Cu  $K_{\alpha}$  source) to check crystallographic  
23 phases present after ball-milling. Microstructural characterization was carried out by  
24 Optical Microscopy (OM, Nikon Eclipse LV150NL) and Scanning Electron Microscopy  
25 (SEM, Zeiss EVO 50), after sample mounting and polishing. SEM micrographs were  
26 mainly taken detecting Backscattered Electrons (BSE), which highlight presence and

1 shape of Al and Sn phases thanks to their Z-contrast. In addition, Energy Dispersive  
2 Spectrometry (EDS) was used to check composition pointwise. analysis According to  
3 Underwood[21], if the volume fraction of porosity is assumed equal to its area fraction, the  
4 mean value of the porosity measured on 5 OM images at 100x magnification, each having  
5 area of about 1.2 mm<sup>2</sup>, was considered; for this purpose, ImageJ open source  
6 software[22] was used. As far as the thermal characterization of PCM is concerned,  
7 Differential Scanning Calorimetry (DSC) analyses were performed to evaluate energy  
8 stored and released during thermal cycles, as usually done for PCMs. DSC tests were  
9 conducted on 55 mg samples obtained from central regions of cylinders in different  
10 processing conditions and after simulated service, using Setaram TG/DSC Labsys 1600.  
11 DSC test cycle consisted in heating at 20°C/min with a holding time of 5 min at 320°C,  
12 cooling at 20°C/min to 40°C, 5 min holding, the cycle being repeated. Finally, mechanical  
13 properties were evaluated by Vickers microhardness tests with load of 4.9 N and dwell  
14 time of 15 s, using Future-tech FM-700 microhardness tester.

15

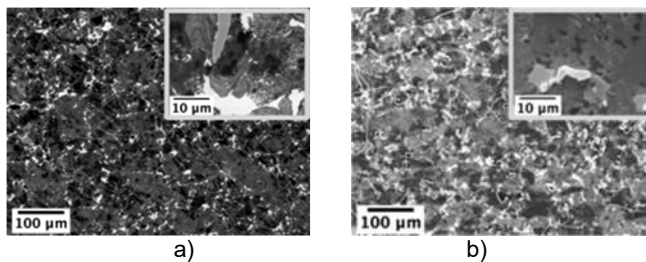
### 16 **3. Results**

#### 17 **3.1 Microstructure**

18 SEM-BSE images of samples obtained using the same process conditions, i.e.  
19 compression at 220°C, but containing different Sn-powder type (106 or SN) are shown in  
20 Figure 2. At low magnification, both samples show coarse homogeneous Sn particles  
21 ranging from a few microns to about 20 µm (bright), coarse Al-rich particles (darker) and  
22 regions of intermediate colour; in high magnification micrographs (Figure 2), the  
23 intermediate regions can be resolved as nanometric particles of Sn and Al. Stationary EDS  
24 analysis in relevant points confirmed the phase compositions inferred from SEM-BSE  
25 micrographs. In the sample HC220 produced with SN powder (Figure 2b), the presence of  
26 bright hair-like structures is observed; their thickness is a few microns, while their length

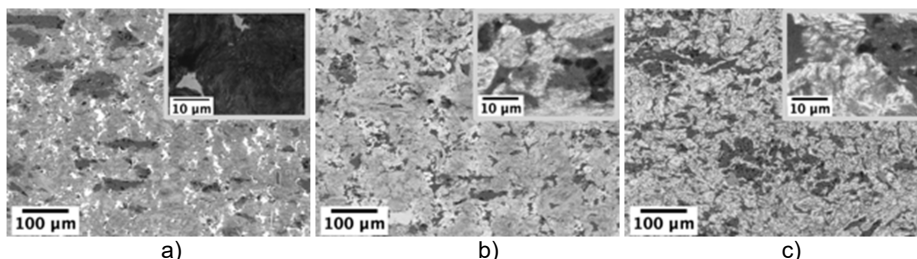


1 ranges between 10  $\mu\text{m}$  and a few hundreds of microns. They are identified as Sn  
 2 whiskers, which formed after sample preparation for micrographic analysis. Although in  
 3 minor quantity, they can be found also in other samples, despite the Sn powder type and  
 4 the compression temperature; they seem to be absent in sintered samples. Samples  
 5 obtained from 106-type Sn powders have just slightly coarser Sn-particles, but most of the  
 6 remaining microstructural features are close to those of samples produced by SN  
 7 powders. The limited effect of Sn powders selected to produce Al-Sn PCM via ball-milling,  
 8 previously noticed in cold compressed samples [20], is here confirmed and is also  
 9 reflected in close thermal and mechanical response. Therefore, samples produced with  
 10 both powders will be here alternatively displayed and quantitative test results were  
 11 averaged.



12  
 13  
 14 *Figure 2. SEM-BSE micrographs of samples compressed at 220°C using different Sn-powder*  
 15 *types (106 for a and SN for b). Compression direction during compaction process: vertical. Higher*  
 16 *magnification micrographs are shown in boxes at top right corner of each image*

17 Some representative microstructures of the samples compressed at 240°C, as-compacted  
 18 and after sintering at 250°C and 500°C, are presented in Figure 3.

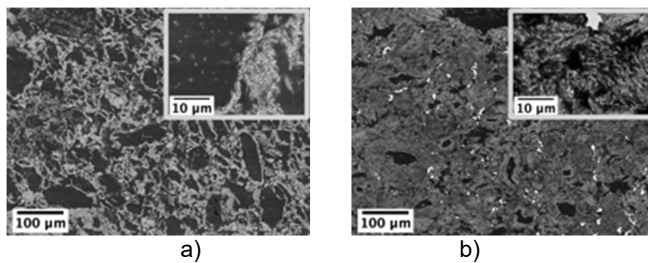


19  
 20  
 21 *Figure 3. SEM-BSE micrographs of samples compressed at 240°C and possibly sintered for 1 hour*  
 22 *at different temperatures; from left to right, no sintering (a), sintering at 250°C (b), sintering at*

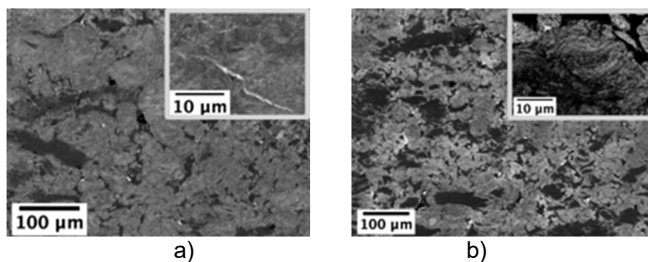
1        500°C (c). Compression direction during compaction process: vertical. Higher magnification  
 2        micrographs are shown in boxes at top right corner of each image

3        The same microstructural features observed in HC220 sample are present in the HC240  
 4        samples. However, it can be noticed that after sintering (Figure 3, b and c) there are no  
 5        more micrometric homogeneous Sn particles and Sn is present only as nanometric  
 6        particles in the in the light grey zone. From a visual analysis of sample surfaces at the end  
 7        of production process, it was observed that no leakage occurred during hot compression,  
 8        while a little leakage occurred during sintering.

9        After 100 thermal cycles carried out between 175 and 285°C to simulate service, visual  
 10       analysis of sample surfaces revealed that leakage of Sn occurred for not-sintered  
 11       samples, while sintered samples had no further Sn losses. Microstructural changes  
 12       occurred in the above materials during simulated service can be appreciated comparing  
 13       the previous microstructures to those presented in Figure 4 and Figure 5, taken at the  
 14       same magnification and with vertical compression direction during densification.



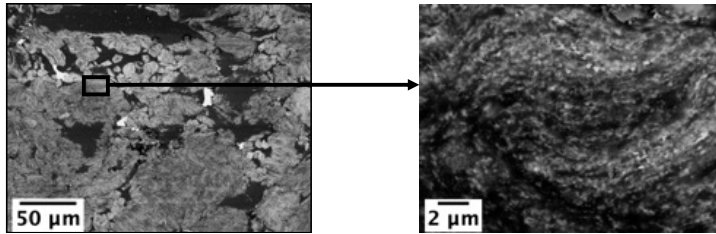
15  
 16  
 17        *Figure 4. SEM-BSE micrographs of not-sintered samples, after 100 cycles; from left to right,*  
 18        *HC220 (a) and HC240 (b). Compression direction during compaction process: vertical. Higher*  
 19        *magnification micrographs are shown in boxes at top right corner of each image*



20  
 21  
 22        *Figure 5. SEM-BSE micrographs of samples compressed at 240°C and sintered, after 100 cycles.*  
 23        *From left to right, sintering at 250°C and at 500°C for 1 hour. Compression direction during*

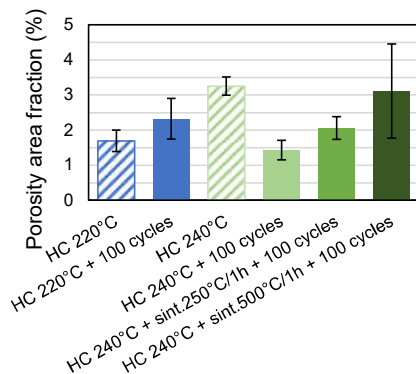
1 compaction process: vertical. Higher magnification micrographs are shown in boxes at top right  
2 corner of each image

3 The microstructure evolution involves the reduction of pure Sn coarse particles and the  
4 increase of the intermediate grey region consisting of nanometric particles of Sn and Al.  
5 These last features can be better observed in high-magnification micrograph in Figure 6;  
6 the microstructure is so fine that using Scanning Electron Microscopy is not possible to  
7 focus these small particles.



8  
9 Figure 6. SEM-BSE image of Sn-rich region in sample compressed at 240°C and sintered at  
10 500°C, after 100 cycles

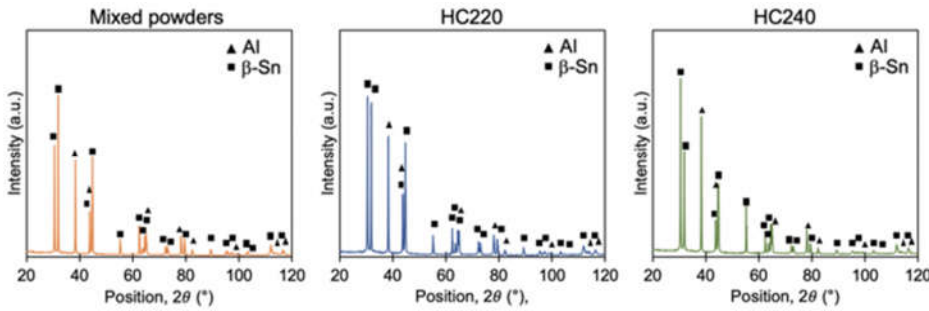
11 The measured porosity area fractions for different process conditions is summarized in  
12 Figure 7. A generally high data scattering can be observed. This is due to difficulties in the  
13 evaluation (either automatic and manual) of porosities in such fine 2-phase microstructures  
14 which displays, both in OM and SEM micrographs, a darker phase (Sn using OM and Al  
15 using SEM) with features close to the small discontinuities. Therefore, a clear trend of  
16 porosity evolution with thermal treatments and thermal cycles could not be identified.



17  
18 Figure 7. Porosity area fraction (%) for different process conditions

1 **3.2 XRD analysis**

2 The XRD analysis was carried out on as milled powders as well as on HC samples  
 3 obtained from BM Al+SN powders compressed below and above Sn melting temperature  
 4 (at 220°C and 240°C) to check which phases were present. The results (Figure 8)  
 5 demonstrate that there are no other phases in addition to pure Al and pure  $\beta$ -Sn, neither in  
 6 mixed powders nor in HC samples. Moreover, after hot compression, peaks do not show  
 7 significant broadening with respect to powders. **On the other hand, changes in peak**  
 8 **intensities are observed in the different conditions, especially for tall peaks at low angle.**



9  
 10 *Figure 8. X-ray diffractogram of mixed powders, HC220 and HC240 samples in the as-compacted*  
 11 *condition*

12 **3.3 Differential Scanning Calorimetry**

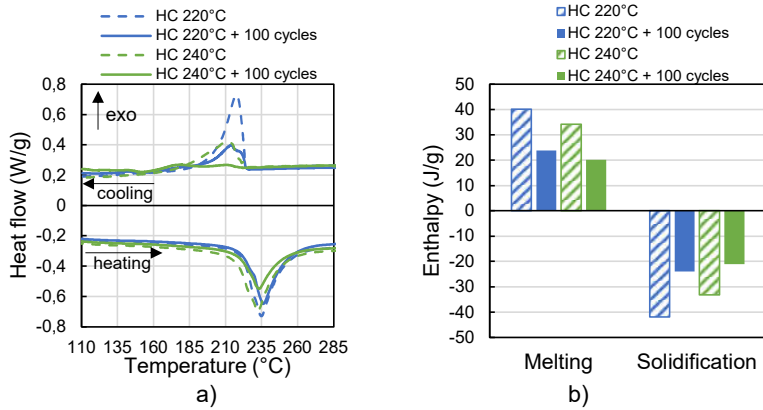
13 The results of DSC tests, presented both in terms of heat flow vs. temperature curves and  
 14 of enthalpies of melting and solidification, are summarized in Figure 9, Figure 10 and **Table**  
 15 **2** for samples tested before and after thermal cycles simulating service.

Compression	Sintering	100 cycles	Measured enthalpy (J/g)		Transition onset temperature (°C)		Transition peak temperature (°C)	
			Melting	Solidification	Melting	Solidification	Melting	Solidification
HC220	-	-	40.20	-41.91	150.56	221.07	235.42	213.72
HC220	-	yes	23.84	-24.04	183.38	223.56	233.34	217.93
HC240	-	-	34.17	-33.16	157.56	221.98	233.52	212.04
HC240	-	yes	20.15	-21.07	160.05	224.94	233.12	178.17
HC240	250°C/1h	yes	18.76	-19.11	164.01	218.22	235.70	193.48
HC240	500°C/1h	yes	24.77	-26.58	154.33	220.00	230.99	208.42

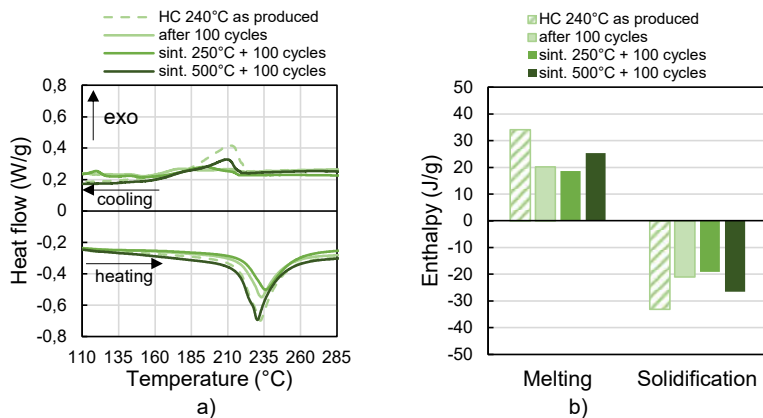
16 *Table 2. Measured enthalpy and transition temperature of all the tested samples in as-produced*  
 17 *conditions and after thermal cycles simulating service*

1 In Figure 9a, the comparison is between different compaction conditions: HC220 and  
2 HC240. Before thermal cycles, sample HC220, compacted just below the melting  
3 temperature of pure Sn and the eutectic Al-Sn temperature, displayed a clear single peak  
4 both in melting and in solidification, with an undercooling of at least 10°C for the latter. For  
5 the specimen HC240, compacted above the melting temperature of pure Sn, only slight  
6 difference in melting peak is observed, while the solidification peak extends and broadens  
7 toward low temperatures. The broadening toward low temperatures as well as the  
8 presence of multiple thermal events in solidification characterize the above samples after  
9 thermal cycles simulating service, where maximum temperature reached is 285°C. Figure  
10 9b summarizes the melting/solidification enthalpy derived from DSC curves in Figure 9a.  
11 Notwithstanding the different shape of peaks in melting/solidification, for each sample the  
12 corresponding enthalpy are almost the same. Moreover, a reduction of transition enthalpy  
13 with respect to the as-compacted samples is observed for all conditions after thermal  
14 cycles.

15 Figure 10 focuses on the effect of sintering temperature and thermal cycling on samples  
16 compacted at 240°C. Figure 10a shows that the presence of broad and/or multiple  
17 solidification peaks is still observed after 100 cycles simulating service and the shape of  
18 thermal events still depends on the sintering condition. Figure 10b once again shows that,  
19 also in this set of samples, the enthalpy in melting and solidification corresponds for each  
20 sample. Further, it is clear that the sample sintered at 500°C kept relatively high enthalpy  
21 after simulated service, compared to the as-compacted sample.



1  
2  
3 *Figure 9. DSC curves (a) and specific enthalpy values (b) for samples produced in different*  
4 *compression conditions (HC220, HC240), before and after thermal treatment and cycles. The*  
5 *specific enthalpy values are the mean values of the results obtained for the two Sn-powder types.*

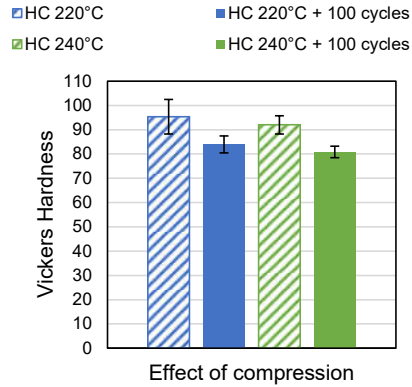


6  
7  
8 *Figure 10. DSC curves (a) and specific enthalpy values (b) for sample produced by HC240 and*  
9 *possibly sintered at 250°C and 500°C, before and after thermal treatment and cycles. The specific*  
10 *enthalpy values are the mean values of the results obtained for the two Sn-powder types.*

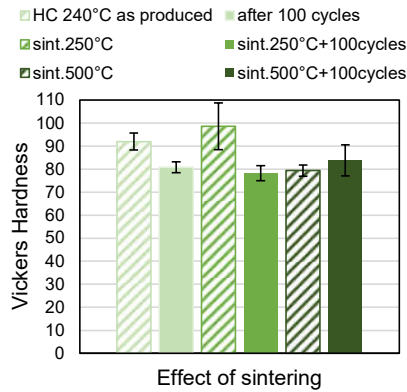
11 **3.4 Mechanical behaviour**

12 Vickers hardness results for samples in different as-compacted conditions are presented in  
13 Figure 11. Generally, simulated service only slightly reduced the hardness of all as-  
14 compacted samples. The effect of heat treatment is presented in Figure 12 for the  
15 representative case of the PCM compacted at 240°C; sintering at 500°C slightly reduced  
16 the mechanical response of the PCM, but the hardness of the sample sintered at this

1 temperature is stable after simulated service. On the contrary, sintering at 250°C slightly  
 2 increases hardness, but this reduced after simulated service.



3  
 4 *Figure 11. Vickers hardness values for samples produced in different compression conditions (CC,*  
 5 *HC220, HC240), before and after thermal treatment and cycles*



6  
 7 *Figure 12. Vickers hardness values for sample produced by HC240 and possibly sintered at 250°C*  
 8 *and 500°C, before and after thermal treatment and cycle*

9  
 10 **4. Discussion**

11 As far as the microstructure is concerned, also in the case of hot compression, the effect  
 12 of Sn-powder type is limited to the residual presence of some slightly coarser Sn particles  
 13 in samples produced using the most heterogeneous Sn powder referred as 106, while

1 most of the volume of the form-stable PCMs produced was characterized by the phase  
2 refinement and homogenization brought about by ball milling.

3 The results from XRD allow to state that the high pressures arisen during ball milling did  
4 not induce phase transformations of Sn from  $\beta$ -phase (stable at atmospheric pressure) to  
5  $\gamma$ - and  $\sigma$ -phases, reported to be stable at pressures higher than 9.4 GPa and 45 GPa,  
6 respectively [23]. Moreover, the presence of other elements as impurities did not induce  
7 the formation of other phases, thus thermal and mechanical behaviour of the material can  
8 be ascribed to the microstructure of the Al-Sn alloy only. **The different intensity of low-  
9 angle peaks in XRD pattern (Figure 8) is attributed to a texture effect due to the powder  
10 metallurgy process. As a matter of fact, this production process does not induce a  
11 preferential orientation of grains, therefore peaks XRD patterns can change in intensity  
12 from sample to sample, especially if produced with different processes.**

13 Considering Sn whiskers, they usually appear randomly in electronic components made of  
14 metals like Sn, Zn and Cd, causing short circuits when they become long enough [24].  
15 According to Chason et al. [24], they are probably due to residual stresses in the metallic  
16 layer, but up to now their occurrence is not predictable and a general effective approach to  
17 suppress their formation is still necessary. In the case of ball-milled PCMs, the production  
18 process can easily cause residual stresses in the material, especially in samples  
19 compressed below Sn melting temperature and in non-sintered samples. They can cause  
20 Sn losses, if they detach or if they melt, nevertheless the amount of Sn which could be  
21 removed by this process is limited to that located very close to surface.

22 Compaction of ball-milled powders just below or above the melting temperature of Sn and  
23 the very close eutectic horizontal line caused a slight change in microstructure as well as  
24 in thermal response. With reference to phase diagram in Figure 1, it can be suggested that  
25 during hot compression at 240°C the external part of coarse Sn particles and part of the  
26 finer ones interact with Al to reach equilibrium composition and, during solidification,



1 transforms in a fine Al+Sn eutectic structure (99.45 mass% Sn [25]) at the boundary of Sn  
2 particle. The presence of a phase with eutectic composition could be the cause of the  
3 undefined boundaries between Al and Sn particles. However, this feature is observed also  
4 in the samples compressed at 220°C, i.e. below eutectic temperature, also before thermal  
5 cycles simulating service. A possible explanation could be the fact that during hot  
6 compression the alloy is subjected to high pressures, which can change the equilibrium  
7 conditions. A concurrent increase of temperature inside the die could have occurred during  
8 compaction, leading the material to the reaction temperature.

9 Eutectic structure is characterized by melting enthalpy of (60.84 J/g [26]), slightly higher  
10 than that of pure tin (59.58 J/g [12]). The presence of eutectic structure is not sufficient to  
11 justify the measured enthalpy of samples HC220 and HC240, slightly higher than the ones  
12 that can be calculated for Al-40Sn mass%, i.e. 23,6 J/g, and this suggest a local  
13 enrichment in Sn of the investigated DSC samples. **On the other hand, the reduction of  
14 measured enthalpy after simulated service is attributed to Sn losses due to leakage during  
15 thermal cycles or sintering. In addition, sub-micrometric particles could have a latent heat  
16 significantly lower than the value for bulk material, as demonstrated by Jiang et al. [27].  
17 Therefore, since the presence of the fine microstructure with sub-nanometric particles  
18 increases with thermal cycle and coarse Sn particles reduce simultaneously, it is possible  
19 that small particles contribute to latent heat reduction. However, this explanation has still to  
20 be verified.**

21 The DSC analyses revealed a specific thermal response of the ball milled Al-Sn alloys that  
22 could be interesting for the use of FS-PCM in specific TES components. This response  
23 was not observed in simple materials with the same chemical composition produced by  
24 compaction of simple mixed powders [16]. As a matter of fact, due to the nanometric size  
25 of Sn particles, solidification is completed at lower temperatures, i.e. undercooling occurs.  
26 The transition toward lower and broader solidification peaks is more evident for the hot

1 compacted samples cycled to simulate service. The Sn solidification in nanometric  
2 particles trapped inside the material and a corresponding undercooling during solidification  
3 is more evident in samples sintered at 500°C. The changes induced in the release of  
4 thermal energy during solidification are an interesting feature from the perspective use of  
5 the PCM for thermal management. As a matter of fact, specific components could benefit  
6 from a fast heat storage at relatively high temperature and by its slower energy release  
7 over a relatively wide temperature range.

8 The distribution of Sn particles has also another effect, the possibility to prevent leakage of  
9 the active phase when it is molten. This fact has been demonstrated by the macroscopic  
10 absence of leakage from sintered samples and it is responsible for the  
11 melting/solidification enthalpy of the PCMs sintered at 500°C relatively stable over cycles  
12 simulating service. Moreover, the values obtained for Vickers hardness are in the same  
13 range as in other ball-milled Al-Sn alloys, i.e. about 80-90 HV, which are higher than the  
14 values for cast Al-Sn alloys, about 30 HV [18], and simple-mixed PCMs, about 30-40 HV  
15 [16].

16 As a result, among the investigated samples, the most promising Al-Sn form-stable PCMs  
17 are those produced by ball-milled powders sintered at 500°C with relatively stable  
18 microstructures, energy storage/release, hardness and negligible leakage.

## 19 **5. Conclusions**

- 20 1. Al-40Sn mass% samples produced by hot compression at 220 and 240°C of ball-  
21 milled Al-Sn mixed powders show minor effects of the initial size distribution of Sn  
22 powders.
- 23 2. Hot compressed specimens were characterized by fine microstructural features and  
24 by the presence of only pure Al and pure  $\beta$ -Sn phase. A phase with almost eutectic  
25 composition starts forming during the hot compression. Microstructural features

1 become finer both after sintering processes at 250°C and 500°C and/or after  
2 simulated service by means of 100 cycles between 175 and 285°C.

3 3. In all the investigated conditions, the material hardness ranged approximately  
4 between 80 and 100 HV and the volumetric porosity was less than 4%. The material  
5 hardness, related to fine microstructural features, is almost twice that of alloys with  
6 the same nominal compositions but coarser structures, produced by compacting  
7 and sintering under the same conditions simple mixed Al and Sn powders,  
8 previously investigated by the research group.

9 4. The thermal response of the Al-40Sn mass% FS-PCM was characterized by close  
10 melting/solidification enthalpies, ranging between 20 and 40 J/g. The highest  
11 values, those of samples hot compressed below the melting temperature of pure  
12 Sn, were also the less stable, due to microstructural changes and possible Sn  
13 losses. Samples hot compressed at 240°C displayed a better thermal stability.  
14 Among them, those further sintered at 500°C were the most stable both from a  
15 thermal and mechanical point of view. During active-phase transition, the fine  
16 microstructure of these FS-PCMs is able to prevent Sn leakage and to have  
17 suitable thermal response, consisting in a relatively fast thermal storage and a  
18 slower heat release.

## 20 **Acknowledgements**

21 The authors would like to thank for their help in characterization tests Paola Bassani,  
22 Enrico Bassani and Maxime Perrin.

23 This work was supported by the Italian Ministry for Education, University and Research  
24 through the project Department of Excellence LIS4.0 (Integrated Laboratory for  
25 Lightweight e Smart Structures).

1 **Author contributions**

2 Chiara Confalonieri: Investigation, Formal analysis, Writing – Original Draft, Writing –  
3 Review and Editing. Aldo Tommaso Grimaldi: Investigation, Writing – Review and Editing.  
4 Elisabetta Gariboldi: Conceptualization, Methodology, Investigation, Writing – Review and  
5 Editing.

6  
7 **Declarations of interest**

8 None.

9  
10 **Data availability**

11 The raw data required to reproduce these findings cannot be shared at this time as the  
12 data also forms part of an ongoing study. The processed data required to reproduce these  
13 findings cannot be shared at this time as the data also forms part of an ongoing study.

14  
15 **References**

- 16 [1] M. Kuta, D. Matuszewska, T.M. Wójcik, The role of phase change materials for the  
17 sustainable energy, E3S Web Conf. 10 (2016) 68.  
18 doi:10.1051/e3sconf/20161000068.
- 19 [2] T. Fiedler, A.J. Rawson, H. Sugo, E. Kisi, Thermal capacitors made from Miscibility  
20 Gap Alloys (MGAs), in: WIT Trans. Ecol. Environ., WIT Press, 2014: pp. 479–486.  
21 doi:10.2495/ESUS140411.
- 22 [3] N. Navarrete, A. Gimeno-Furio, R. Mondragon, L. Hernandez, L. Cabedo, E.  
23 Cordoncillo, J.E. Julia, Nanofluid based on self-nanoencapsulated metal/metal alloys  
24 phase change materials with tuneable crystallisation temperature, Sci. Rep. 7 (2017)  
25 17580. doi:10.1038/s41598-017-17841-w.

- 1 [4] S. Reed, H. Sugo, E. Kisi, High temperature thermal storage materials with high  
2 energy density and conductivity, *Sol. Energy*. 163 (2018) 307–314.  
3 doi:10.1016/J.SOLENER.2018.02.005.
- 4 [5] H. Nazir, M. Batool, F.J. Bolivar Osorio, M. Isaza-Ruiz, X. Xu, K. Vignarooban, P.  
5 Phelan, Inamuddin, A.M. Kannan, Recent developments in phase change materials  
6 for energy storage applications: A review, *Int. J. Heat Mass Transf.* (2019).  
7 doi:10.1016/j.ijheatmasstransfer.2018.09.126.
- 8 [6] J.Q. Sun, R.Y. Zhang, Z.P. Liu, G.H. Lu, Thermal reliability test of Al–34%Mg–6%Zn  
9 alloy as latent heat storage material and corrosion of metal with respect to thermal  
10 cycling, *Energy Convers. Manag.* 48 (2007) 619–624.  
11 doi:10.1016/J.ENCONMAN.2006.05.017.
- 12 [7] G. Wei, G. Wang, C. Xu, X. Ju, L. Xing, X. Du, Y. Yang, Selection principles and  
13 thermophysical properties of high temperature phase change materials for thermal  
14 energy storage: A review, *Renew. Sustain. Energy Rev.* 81 (2018) 1771–1786.  
15 doi:10.1016/J.RSER.2017.05.271.
- 16 [8] S.A. Mohamed, F.A. Al-Sulaiman, N.I. Ibrahim, M.H. Zahir, A. Al-Ahmed, R. Saidur,  
17 B.S. Yılbaş, A.Z. Sahin, A review on current status and challenges of inorganic  
18 phase change materials for thermal energy storage systems, *Renew. Sustain.*  
19 *Energy Rev.* 70 (2017) 1072–1089. doi:10.1016/J.RSER.2016.12.012.
- 20 [9] C. Zhou, S. Wu, Medium- and high-temperature latent heat thermal energy storage:  
21 Material database, system review, and corrosivity assessment, *Int. J. Energy Res.*  
22 43 (2019) 621–661. doi:10.1002/er.4216.
- 23 [10] J. Paris, M. Falardeau, C. Villeneuve, Thermal Storage by Latent Heat: A Viable  
24 Option for Energy Conservation in Buildings, *Energy Sources*. 15 (1993) 85–93.  
25 doi:10.1080/00908319308909014.

- 1 [11] W. Su, J. Darkwa, G. Kokogiannakis, Review of solid–liquid phase change materials  
2 and their encapsulation technologies, *Renew. Sustain. Energy Rev.* 48 (2015) 373–  
3 391. doi:<https://doi.org/10.1016/j.rser.2015.04.044>.
- 4 [12] W. Shackelford, James F., Alexander, ed., *CRC Materials Science and Engineering*  
5 *Handbook*, 3rd ed., CRC Press, Boca Raton, 2001.  
6 doi:<https://doi.org/10.1201/9781420038408>.
- 7 [13] K. Pielichowska, K. Pielichowski, Phase change materials for thermal energy  
8 storage, *Prog. Mater. Sci.* 65 (2014) 67–123. doi:10.1016/J.PMATSCI.2014.03.005.
- 9 [14] H. Sugo, E. Kisi, D. Cuskelly, Miscibility gap alloys with inverse microstructures and  
10 high thermal conductivity for high energy density thermal storage applications, *Appl.*  
11 *Therm. Eng.* 51 (2013) 1345–1350.  
12 doi:10.1016/J.APPLTHERMALENG.2012.11.029.
- 13 [15] X. Liu, M.Q. Zeng, Y. Ma, M. Zhu, Melting behavior and the correlation of Sn  
14 distribution on hardness in a nanostructured Al–Sn alloy, *Mater. Sci. Eng. A.* 506  
15 (2009) 1–7. doi:10.1016/J.MSEA.2008.12.054.
- 16 [16] E. Gariboldi, M. Perrin, *Metallic Composites as Form-Stable Phase Change Alloys*,  
17 in: *THERMEC 2018*, Trans Tech Publications, 2019: pp. 1966–1971.  
18 doi:10.4028/www.scientific.net/MSF.941.1966.
- 19 [17] N.I. Noskova, N.F. Vil'danova, Y.I. Filippov, R. V Churbaev, I.A. Pereturina, L.G.  
20 Korshunov, A. V Korznikov, Preparation, deformation, and failure of functional Al-Sn  
21 and Al-Sn-Pb nanocrystalline alloys, *Phys. Met. Metallogr.* 102 (2006) 646–651.  
22 doi:10.1134/S0031918X06120131.
- 23 [18] X. Liu, M.Q. Zeng, Y. Ma, M. Zhu, Promoting the high load-carrying capability of Al–  
24 20wt%Sn bearing alloys through creating nanocomposite structure by mechanical

- 1 alloying, *Wear*. 294–295 (2012) 387–394. doi:10.1016/j.wear.2012.07.021.
- 2 [19] C. Suryanarayana, Mechanical alloying and milling, *Prog. Mater. Sci.* 46 (2001) 1–  
3 184. doi:[https://doi.org/10.1016/S0079-6425\(99\)00010-9](https://doi.org/10.1016/S0079-6425(99)00010-9).
- 4 [20] C. Confalonieri, Z. Li, E. Gariboldi, Metallic Form-Stable Phase Change Materials for  
5 Thermal Energy Storage and Management: general features and effect of  
6 manufacturing process on thermal response and stability, *La Metall. Ital. - Int. J. Ital.*  
7 *Assoc. Metall.* 7/8 (2019) 12–20.
- 8 [21] E. Underwood, The Mathematical Foundations of Quantitative Stereology, in: G.  
9 Pellissier, S. Purdy (Eds.), *Stereol. Quant. Metallogr.*, ASTM International, West  
10 Conshohocken, PA, 1972: pp. 3–38. doi:10.1520/STP36841S.
- 11 [22] W.S. Rasband, ImageJ, (2018). <https://imagej.net/Welcome>.
- 12 [23] W. Steurer, Crystal Structures of the Elements, *Encycl. Mater. Sci. Technol.* (2001)  
13 1880–1897. doi:10.1016/B0-08-043152-6/00344-2.
- 14 [24] E. Chason, F. Pei, N. Jain, A. Hitt, Studying the Effect of Grain Size on Whisker  
15 Nucleation and Growth Kinetics Using Thermal Strain, *J. Electron. Mater.* 48 (2019)  
16 17–24. doi:10.1007/s11664-018-6594-x.
- 17 [25] A.J. McAlister, D.J. Kahan, The Al–Sn (Aluminum-Tin) System, *Bull. Alloy Phase*  
18 *Diagrams.* 4 (1983) 410–414. doi:10.1007/BF02868095.
- 19 [26] B. Predel, Al–Sn (Aluminum-Tin): Datasheet from Landolt-Börnstein - Group IV  
20 Physical Chemistry · Volume 5A: “Ac–Au – Au–Zr” in SpringerMaterials, 5A (1991).  
21 doi:10.1007/10000866\_144.
- 22 [27] B. Yang, Y. Gao, C. Zou, Q. Zhai, E. Zhuravlev, C. Schick, Size-dependent  
23 undercooling of pure Sn by single particle DSC measurements, *Chinese Sci. Bull.* 55  
24 (2010) 2063–2065. doi:10.1007/s11434-010-3041-7.

1

2